Supplementary Material

An experimental study of flow near an advancing contact line: a rigorous test of theoretical models

C. Gupta, A. Choudhury, L. D. Chandrala and H. N. Dixit

In this document, quantitive data from PIV experiments and a `MATLAB` code are provided which can be downloaded from here. We hope this data will facilitate numerical and theoretical modeling groups to develop more sophisticated moving contact line models based on our experiments. A comparison of the observed dynamic contact angle in the experiments is also shown against predictions from popular models. Our data is directly contrasted against similar measurements carried out by [1] for a drop moving on an inclined plate.

S1 Flow fields

One of the goals of the paper is to provide quantitative data from the experiments which can be used to generate and test sophisticated moving contact line models. To enable this, it is necessary to provide quantitative information about the flow fields.

The flow fields are obtained by analyzing the particle images captured after the flow achieves a steady state. Sample streakline images are shown in figure S1 for flow in a transient state and in a steady state. In the transient state, the streaklines are found to cross each other, and occurs at the start of the experiment by the impulsive motion of the plate. For very viscous fluids, the transient state is very short and steady-state motion is achieved quickly.

Figure S2 shows vector fields obtained from PIV measurements for 500 cSt, 100 cSt, 20 cSt, and 10 cSt silicone oils respectively. A comparison of the experimental data with MWS theory is also shown in figure S3 at $Re = 0.023$ and $Ca = 6.77 \times 10^{-5}$. To obtain a precise comparison, it is to be noted that the direction of the vectors and corresponding magnitude should match between experiments and theory. To determine the region where the theory best agrees with the experiments, we define a spatial error as follows:

$$\mathcal{E}(x) = \sqrt{\frac{\sum_i^N \left(\mathbf{u}_{\text{exp}} - \mathbf{u}_{\text{th}}\right)^2}{N}}\Bigg|_{u \in \text{ points in shaded region}} \tag{S1}$$

where $\mathbf{u}_{\text{exp}}$ and $\mathbf{u}_{\text{th}}$ refer to the non-dimensional total velocity in experiments and MWS theory respectively. The RMS difference between the experiments and theory is calculated inside the shaded region shown in figure S4(a) and normalised with the number of vector points, N. The

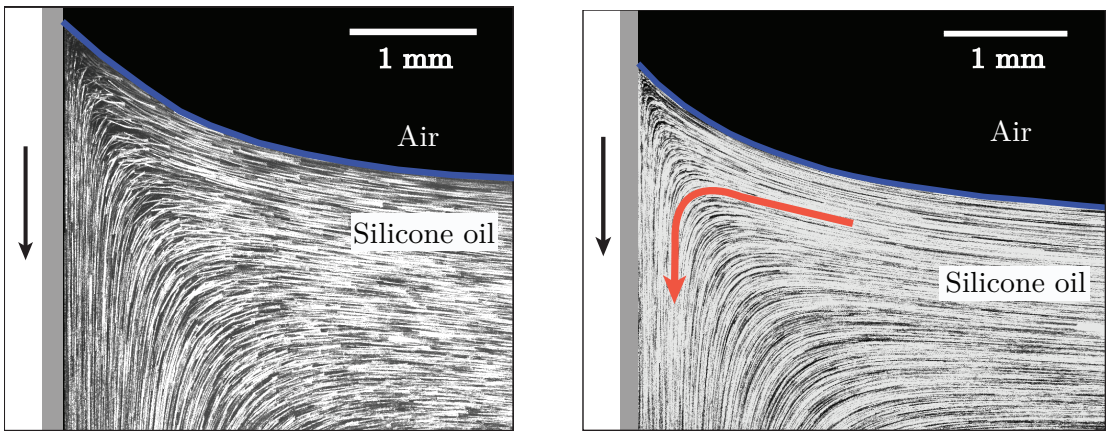

(a) (b)

Figure S1: A sample image of streaklines in the bulk near a moving contact line (a) a transient situation in the flow (b) a flow situation after reaching steady state.

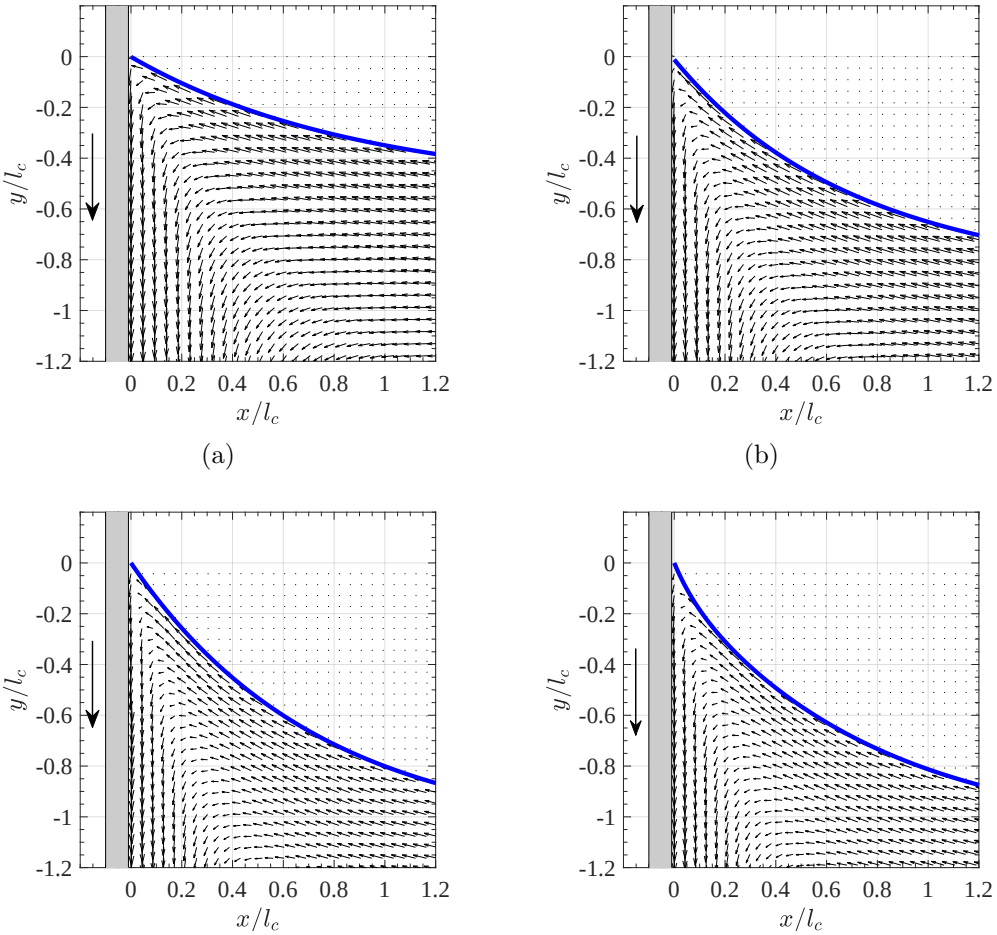

(a) (b)

(c) (d)

Figure S2: Non-dimensional flow fields: (a) Silicone 500 cSt at $Re = 1.3 \times 10^{-3}$ and $Ca = 1.4 \times 10^{-2}$, (b) Silicone 100 cSt at $Re = 7.7 \times 10^{-3}$ and $Ca = 2.41 \times 10^{-3}$, (c) Silicone 20 cSt at $Re = 1.15 \times 10^{-2}$ and $Ca = 1.36 \times 10^{-4}$, (d) Silicone 10 cSt at $Re = 0.023$ and $Ca = 6.77 \times 10^{-5}$. Here, a blue solid curve represents an interface that separates the oil from the air phase. The gray slab is the solid surface that is moving vertically downwards into the oil bath, as shown by the arrow.

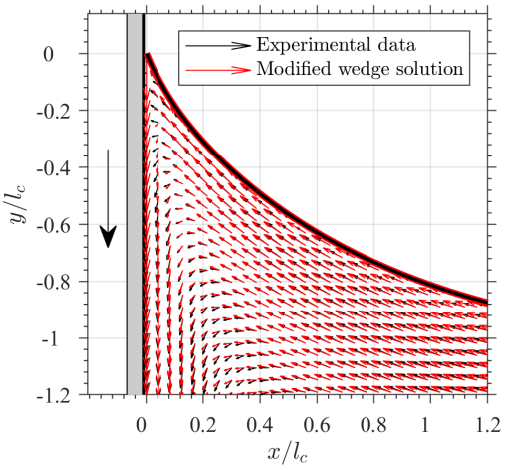

Figure S3: A comparison of flow fields between experiments and modulated wedge solution for 10 cSt Silicone oil at $Re = 0.023$ and $Ca = 6.77 \times 10^{-5}$. The black arrows represent experimental flow fields and the red arrows represent modulated wedge solution. The comparison is carried out by estimating the theoretical flow fields over the cartesian grids of the experiments.

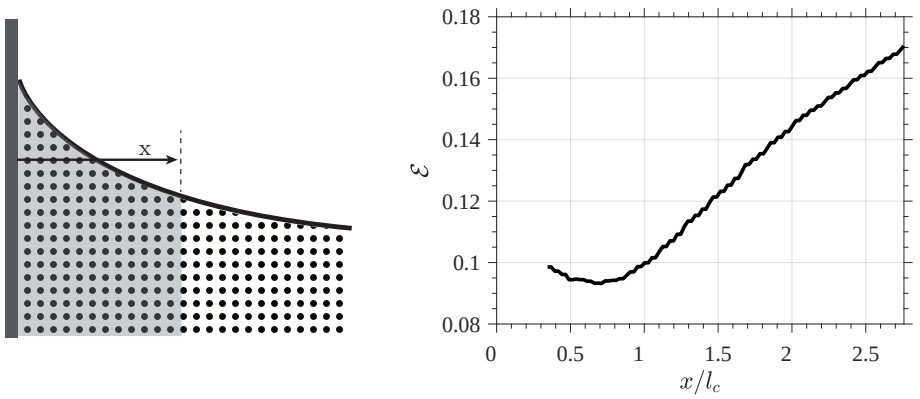

(a) (b)

Figure S4: (a) Measuring the error between experiments and theory. Error, $\mathcal{E}(x)$, is a measure of the deviation between experiments and theory for all grid points inside the shaded region. (b) Variation of the error in the domain for 10 cSt Silicone oil at $Re = 0.023$ and $Ca = 6.77 \times 10^{-5}$.

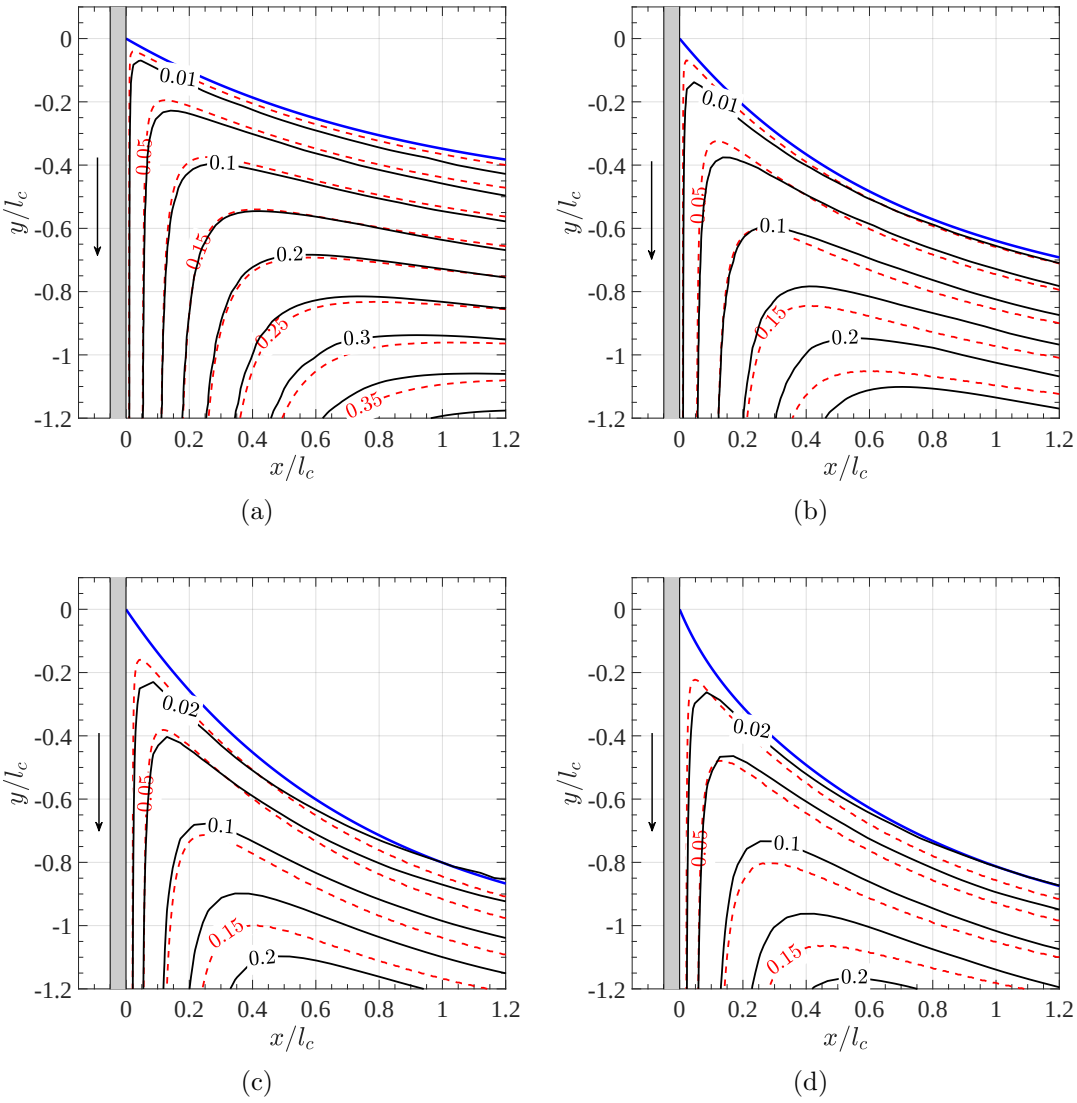

Figure S5: Contours of non-dimensional streamfunction obtained from experiments and viscous theory. The gray rectangle represents the solid plate moving downwards, and the blue solid curve represents the interface between air and silicone oil. Experimental streamfunction contours (black solid curves) are derived using mass balance considerations from velocity vector field using PIV experiments and the theoretical predictions (red dashed curves) are obtained from viscous theory incorporating the effect of a curved interface. (a) Silicone 500 cSt at $Re = 1.3 \times 10^{-3}$ and $Ca = 1.4 \times 10^{-2}$, (b) Silicone 100 cSt at $Re = 7.7 \times 10^{-3}$ and $Ca = 2.41 \times 10^{-3}$, (c) Silicone 20 cSt at $Re = 1.15 \times 10^{-2}$ and $Ca = 1.36 \times 10^{-4}$, (d) Silicone 10 cSt at $Re = 0.023$ and $Ca = 6.77 \times 10^{-5}$

.

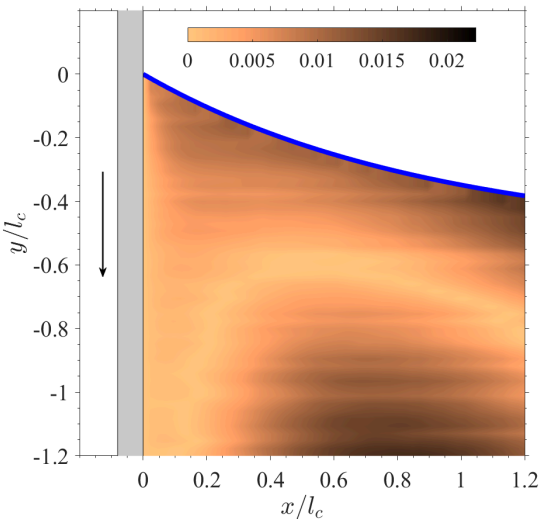

Figure S6: Comparison between experimentally obtained streamfunction contours and theoretical predictions shown in terms of the magnitude of the difference in non-dimensional streamfunction values, $|\psi - \psi_{MWS}|$. The data corresponds to figure S5(a). The interface is shown with a blue solid curve.

extent of the shaded region, x, is increased in each calculation. The error, $\mathcal{E}(x)$, is therefore a direct comparison between experiments and theory. Figure S4(b) shows that the error reaches a minima before eventually increases. This behaviour is understandable since theory is expected to perform poorly with experiments very close to the wall as well as far away from the contact line.

Streamfunction contours are shown in figure S5 corresponding to each vector field plot shown in figure S2. The contour plots show comparisons between experimental data shown in the black solid curves against MWS theory shown in the red dashed curves. To quantify the comparison, the difference between streamfunctions, i.e., $|\psi - \psi_{MWS}|$, is also shown in figure S6 corresponding to 500 cSt silicone oil experimental data.

S2 Dynamic contact angle

In a classical study, Hoffman [2] reported the variation of dynamic contact angle with Ca by pushing different fluids into a capillary tube. We map the Hoffman data using the Cox-Voinov contact angle model as shown in figure S7 where a linear regression fit performs well with the data. The obtained slope in this fit is 81.1 whereas the slope of the data from the present study is 78.7 shown in figure S8(c). This suggests that the Cox-Voinov model performs very well against both sets of experiments and also shows the universal nature dynamic contact angle, irrespective of the widely different geometries in Hoffman's experiments and the present study.

We also evaluate various contact angle models popular in the literature involving experiments with different grades of silicone oils. The contact angle data are mapped onto the $f(\theta_d) - Ca$ plane as shown in figure S8. The contact angles are acute ($\theta_d < 90°$) in all the experiments in the present study. Experiments are mainly performed in the range $10^{-5} < Ca < 10^{-2}$ which covers a wide spectrum of Ca. For fitting the data against different contact angle models, both static

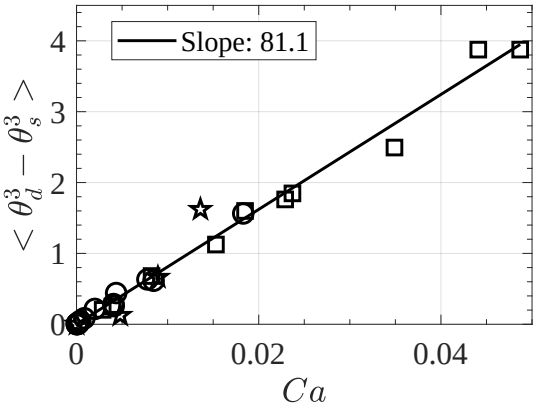

Figure S7: A linear fit of the Cox-Voinov model to Hoffman's data [2].

(θ_s) and dynamic (θ_d) contact angles have to be determined. The static advancing contact angle, $\theta_{s,a}$, is used in place of θ_s. The dynamic contact angle is estimated from the interface shape as discussed in the paper. The resolution of the experiments is the order of a few microns ($\sim 4\mu$m to 8μm) and hence, the actual measurement of the angle is carried out a few microns away from the contact line.

Below, we discuss four different contact angle models. The comparison is similar to what was carried out for viscous drops on an incline by Le Grand *et al.* [1]. Regression analysis is performed by fitting a straight line for different contact angle models as shown in figure S8. The values of the slopes obtained in the present study are directly contrasted against the work of Le Grand *et al.* [1] in table S1.

S2.1 Molecular kinetic model [3]

Blake and Haynes proposed the general form of the model in the cosine terms that are further truncated in the small θ_d limit which is given as:

$$(\theta_d^2 - \theta_s^2) = 2A \cdot Ca \tag{S2}$$

Where A is a constant. For comparison, the truncated form of the model is justified to use as all the data points are at less than 90°. Figure S8(a) shows a linear fit over the experimental data with the slope of 54.3 whereas Le Grand *et al.* [1] reported the slope of 88.11 (see table S1).

S2.2 De Gennes model [4]

The truncated form of the model using small angle approximation is as follows:

$$\theta_d(\theta_d^2 - \theta_s^2) = 6\ln(L/l_s) \cdot Ca \tag{S3}$$

This is a third-order model in contact angle, valid for small angles only. Here L is macroscopic length and l_s is slip length. In eq. S3, '$6\ln(L/l_s)$' is the prefactor in the model. Figure S8(b)

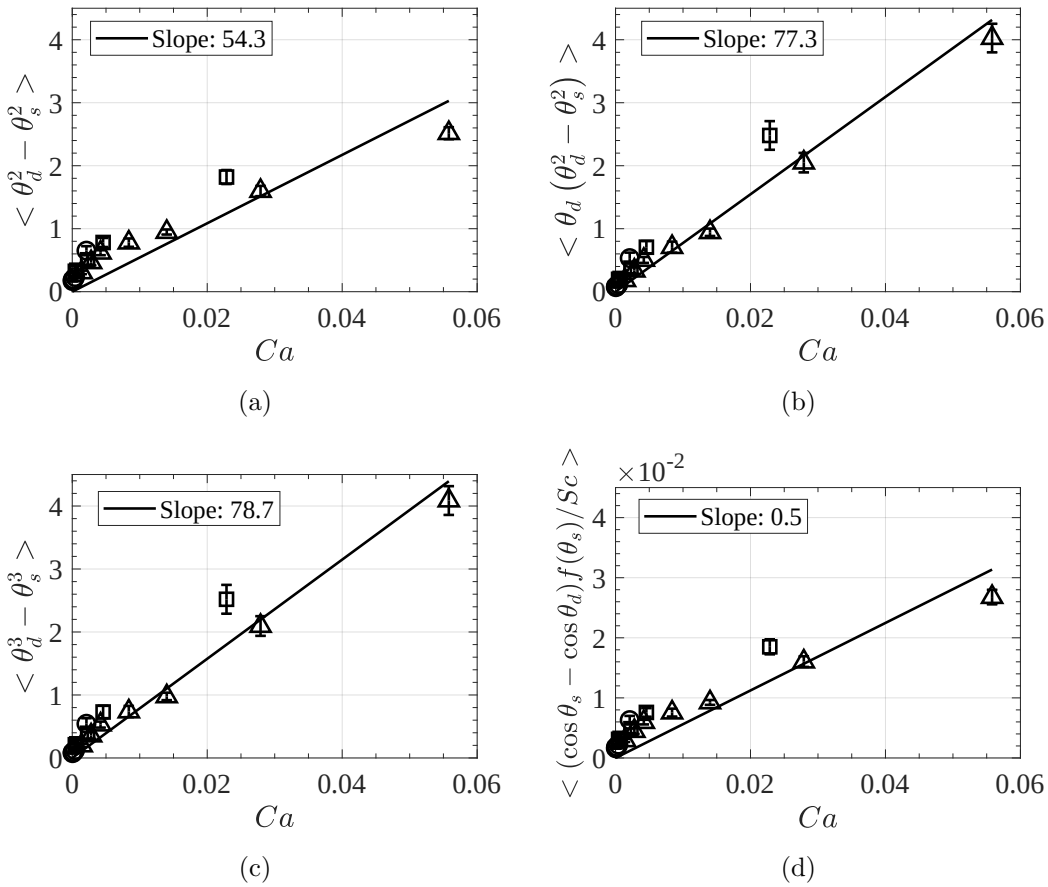

Figure S8: Comparison of several contact angle models for experiments with three different silicone oils: 10 cSt (∘), 100 cSt (□) and 500 cSt (△). (a) Molecular kinetic model, (b) de Gennes model, (c) Cox-Voinov model, (d) Shikhmurzaev model.

	Le Grand *etal.* 2005	Current	Hoffman *etal.* 1975
Molecular kinetic model	88.11	54.3	-
De Gennes model	99.69	77.3	-
Cox-Voinov model	129.57	78.7	81.1
Shikhmurzaev model	-	0.5	-

Table S1: A comparison of slopes obtained from different contact angle models.

shows a linear fit of experimental data points with a slope of 77.3 whereas Le Grand *et al.* [1] reported the slope of 99.69 (see table S1)

S2.3 Cox-Voinov Model [5],[6]

The general form of the model is in the term of $g(\theta)$ which is a function of sine and cosines. The truncated expression of the model is valid for $\theta_d < 3\pi/4$ and given as:

$$\theta_d^3 - \theta_s^3 = 9\ln(L/l_s)\cdot Ca \tag{S4}$$

The truncated form of the model comes out as third order in dynamic contact angle. Figure S8(c) shows a linear fit of experimental data points with a slope of 78.7 whereas Le Grand *et al.* [1] reported the slope of 129.57 (see table S1). Interpreting L as the capillary length-scale, the slip length estimated by this fit is $l_s = 223$ nm.

S2.4 Shikhmurzaev model [7]

All the necessary expressions related to the model are mentioned below:

$$(\cos\theta_s - \cos\theta_d) f(\theta_d)/Sc = Ca \tag{S5}$$

$$f(\theta_d) = \sqrt{\frac{1 + (1-\rho_G^s)\cos\theta_s}{4(\cos\theta_s + B)(\cos\theta_d + B)}} \tag{S6}$$

$$B = \frac{1 + \rho_G^s u_{12}(\theta_d)}{1 - \rho_G^s} \tag{S7}$$

$$u_{12}(\theta_d) = \frac{\sin\theta_d - \theta_d\cos\theta_d}{\sin\theta_d\cos\theta_d - \theta_d} \tag{S8}$$

Here u_{12} is the interfacial speed which is obtained from the study of HS71 [8]. This is the only model that introduces interfacial speed as a part of the model. The important fitting parameters in the model that should be known a priori are Sc and ρ_G^s. The values of the parameters $Sc = 1$ and $\rho_G^s = 0.98$ are directly taken from the study of Puthenveettil *et al.* [9] to estimate the slope of the linear fitting of the experimental data. Figure S8(d) shows a linear fit of experimental data points with a slope of 0.5 (see table S1).

References

[1] Nolwenn Le Grand, Adrian Daerr, and Laurent Limat. Shape and motion of drops sliding down an inclined plane. *J. Fluid Mech.*, 541:293–315, 2005.

[2] Richard L Hoffman. A study of the advancing interface. i. interface shape in liquid—gas systems. *J. Colloid Interface Sci.*, 50(2):228–241, 1975.

[3] TD Blake and JM Haynes. Kinetics of liquidliquid displacement. *J. Colloid Interface Sci.*, 30(3):421–423, 1969.

[4] Pierre-Gilles De Gennes. Wetting: statics and dynamics. *Rev. Mod. Phys.*, 57(3):827, 1985.

[5] OV Voinov. Hydrodynamics of wetting. *Fluid Dyn.*, 11(5):714–721, 1976.

[6] RG Cox. The dynamics of the spreading of liquids on a solid surface. part 1. viscous flow. *J. Fluid Mech.*, 168:169–194, 1986.

[7] Yu D Shikhmurzaev. The moving contact line on a smooth solid surface. *Int. J. Multiph. Flow*, 19(4):589–610, 1993.

[8] Chun Huh and LE Scriven. Hydrodynamic model of steady movement of a solid/liquid/fluid contact line. *J. Colloid Interface Sci.*, 35(1):85–101, 1971.

[9] Baburaj A Puthenveettil, Vijaya K Senthilkumar, and EJ Hopfinger. Motion of drops on inclined surfaces in the inertial regime. *J. Fluid Mech.*, 726:26–61, 2013.